J. Plasma Phys. (2023), *vol*. 89, 175890202
Published by Cambridge University Press
doi:10.1017/S0022377823000260

Observations of dust fragmentations in the Experimental Advanced Superconducting Tokamak

Yang Miao[1], Jian-Sheng Hu[2], Chao Fu[1], Yang Wang[1], Sergey A. Khrapak[3], Fang-Chuan Zhong[1,4] and Cheng-Ran Du[1,4,†]

[1]College of Science, Donghua University, 201620 Shanghai, PR China

[2]Institute of Plasma Physics, Chinese Academy of Sciences, 230031 Hefei, PR China

[3]Joint Institute for High Temperatures, Russian Academy of Sciences, 125412 Moscow, Russia

[4]Member of Magnetic Confinement Fusion Research Centre, Ministry of Education, 201620 Shanghai, PR China

(Received 21 October 2022; revised 8 March 2023; accepted 9 March 2023)

The transport phenomena of dust particles have been widely observed in fusion plasmas. In this article, we report the observations of dust fragmentations in the Experimental Advanced Superconducting Tokamak (EAST). A dust particle splits into two daughter particles and their motions are recorded before and after the breakup with a fast video camera. The trajectories of the daughter particles in the experiment are consistent with equation-of-motion simulations. The stability of a rotating charged particle in the plasma is briefly discussed.

Key words: dusty plasmas

1. Introduction

The interaction between the edge of a fusion plasma and the plasma-facing components (PFCs) is one of the most important issues in fusion (Sharpe, Petti & Bartels 2002; Grisolia *et al.* 2009; Ratynskaia *et al.* 2020; Ratynskaia, Bortolon & Krasheninnikov 2022*a*). The melting of the surface layer on the PFCs and delamination of the co-deposits are considered to be the main reasons for the generation of dust particles. These particles lead to substantial deleterious effects on the discharge performance, including disruption and radiation loss (Liu *et al.* 2013).

In recent years, studies of dust particles in fusion devices have been carried out in many aspects, including the generation and re-deposition of dust particles (Tolias *et al.* 2016; Ratynskaia *et al.* 2016, 2018), the interaction between dust particles and plasma (Laux, Balden & Siemroth 2014; Autricque *et al.* 2018; Block & Melzer 2019), particle injections and transports (Delzanno & Tang 2014; Lunsford *et al.* 2018) and the characteristics of dust particles (Arnas *et al.* 2017; Pardanaud *et al.* 2020; Pan *et al.* 2022). The applications of fast cameras provide an important method for particle and plasma diagnosis (Ratynskaia

† Email address for correspondence: chengran.du@dhu.edu.cn

et al. 2011; Shalpegin *et al.* 2015). It is possible to obtain the particle trajectories from the wall materials to the core plasma.

During their transport, dust particles sample a wide range of plasma conditions (Winter 1999; Fortov *et al.* 2005; Morfill & Ivlev 2009). As one of the most interesting phenomena, fragmentation of dust particles has been observed in tokamaks (Holgate *et al.* 2019). Since the dust fragments are usually small in size and have low heat capacity, their penetration depth from the scrape-off layer (SOL) is correspondingly small. As a result, fragmentation of dust particles leads to lower Z impurities and less Bremsstrahlung in the core and can mitigate the disruptions triggered by localized plasma cooling to some extent. Therefore, understanding the mechanism of fragmentation and the dynamics of fragments is of great importance to control the hazards caused by these dust impurities.

In fusion, the plasma temperature reaches $\sim$1 keV in the core, but drops dramatically in the SOL. Nevertheless, it still exceeds the melting temperature of materials of the PFCs such as tungsten and molybdenum. The dust particles appear as droplets and may undergo an electrostatic breakup into several fragments (Duft *et al.* 2002; Koromyslov, Grigor'Ev & Rybakova 2002; Achtzehn *et al.* 2005). The instability condition of a charged particle in vacuum or neutral gas was derived by Rayleigh (1882) and reads $Q^2 > 16\pi\gamma a^3$, where Q is the particle charge, γ is the liquid surface tension and a is the particle radius. Recent studies show that the particles are more likely to be destroyed due to electrostatic breakup than to slower processes such as evaporation in fusion devices (Coppins 2010; Holgate & Coppins 2018). Rotation is another main cause of fragmentation (Krasheninnikov *et al.* 2004; Liao & Hill 2017; Holgate *et al.* 2019). The particles in plasma rotate with high angular velocities due to various mechanisms. In a low-temperature plasma, the angular velocity can reach up to 10^5 rad s^{-1} (Hutchinson 2004), while in a high-temperature plasma, it can reach up to 10^9 rad s^{-1} due to Lorentz force (Krasheninnikov 2006).

In this article, we report a direct observation of the spontaneous fragmentation of dust particles in the Experimental Advanced Superconducting Tokamak (EAST) using a high-speed camera. Equation-of-motion simulations were performed and the results were consistent with the experimental observations. Finally, the criterion for the fragmentation is briefly discussed.

2. Experimental observations

The EAST is a fully superconducting tokamak device, which aims at implementing long-pulse high-confinement plasma operations (Keilhacker *et al.* 1984; Li *et al.* 2013). The major and minor radii are 1.7 and 0.45 m, respectively. The upper divertor has an actively water-cooled tungsten–copper monoblock structure while the lower divertor is made of graphite. The first wall materials are of molybdenum (Wang *et al.* 2014; Wan *et al.* 2015). In order to study various phenomena in the plasma, a high-speed CCD camera (Phantom V710) has been installed in K port of the EAST with a fixed focal length and aperture (Jia *et al.* 2015; Chen *et al.* 2019). The optical system views the tangential direction of the tokamak and the field of view is designed to be -29° to 29° in vertical orientation and -29° to 18° in horizontal orientation. The data acquisition speed and spatial resolution of the whole system are up to 50 000 frames per second (fps) and 6 mm per pixel, respectively.

Multiple fragmentation events were recorded in the discharge by the high-speed camera. As a typical example observed in discharge shot 46618, a single dust particle travelled with a high velocity in the SOL and broke into two pieces. The two fragments obtained a transverse velocity and further travelled apart, as shown in figure 1. The dust particles appear as bright spots in the dark background in the video with a recording rate of

https://doi.org/10.1017/S0022377823000260 Published online by Cambridge University Press

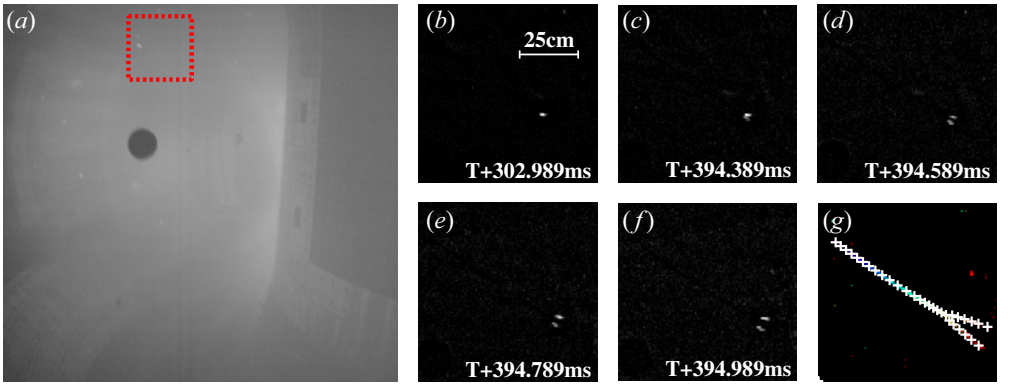

FIGURE 1. A typical fragmentation event of a dust particle recorded in discharge shot 46618 in the EAST. The fragmentation occurred in the region marked by the dotted rectangle in (*a*). The recording rate is 5000 fps. (*b–f*) The particle positions at five consecutive times and (*g*) the full trajectories of the particles before and after the fragmentation. The white crosses represent the results of the particle tracking by the SPIT algorithm.

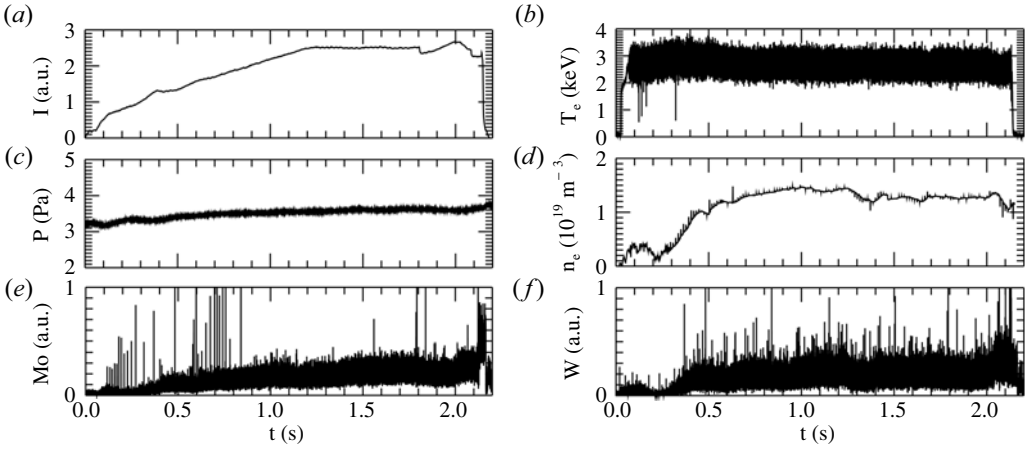

FIGURE 2. The evolution of the plasma parameters including current (*a*), electron temperature (*b*) and density (*d*) in the core, gas pressure (*c*) and emission of molybdenum (*e*) and tungsten (*f*) in discharge shot 46618.

5000 fps. The recorded two-dimensional projected motions were tracked by the simple particle identification and tracking (SPIT) algorithm.

The evolution of the plasma parameters in this discharge is shown in figure 2. The neutral gas pressure is about 3.5 Pa. The toroidal field strength B_t is about 1.85 T. The current increased in the first second and reached a steady state until the disruption at $t \sim 2.2$ s. The average electron density in the core increased relatively fast and reached a plateau of 1.3×10^{19} m^{-3} for the rest of the discharge. The electron temperature was measured by electron cyclotron emission (ECE) and is about 3 keV in the core. Note that the electron temperature and density in the plasma edge (SOL) are much lower than those in the core. Besides, the evolution of the emission of tungsten and molybdenum, corresponding to the divertor and wall materials in the EAST, are shown in figure 2(*e*,*f*).

https://doi.org/10.1017/S0022377823000260 Published online by Cambridge University Press

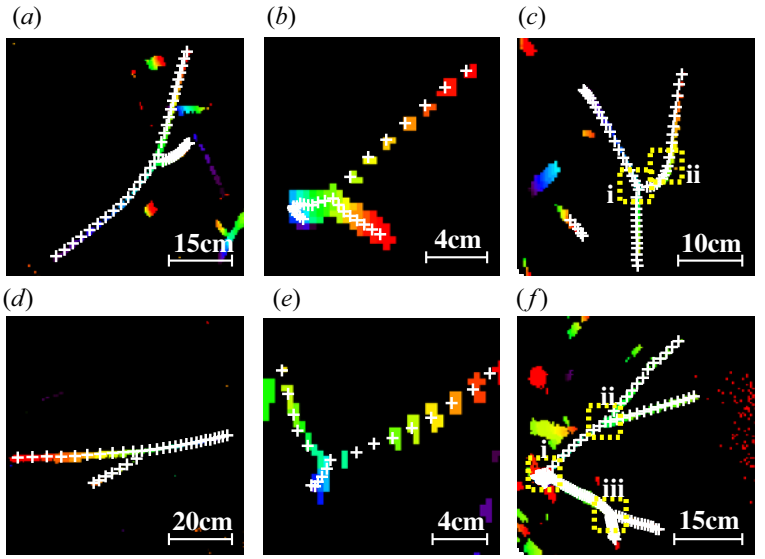

FIGURE 3. A few examples of fragmentation events observed in the EAST. The white plus symbols represent the positions of the dust particles tracked by the SPIT algorithm. Single fragmentation events are shown in (*a*,*b*,*d*,*e*). Multiple fragmentation events are shown in (*c*,*f*), highlighted by the yellow dotted rectangles.

More fragmentation events observed in different discharges in the EAST are shown in figure 3. The dust particles travelled in different directions and with various velocities. Some trajectories, such as shown in figure 3(*a*,*d*), are similar to that shown in figure 1, despite the different initial velocities of the particles and locations of the observations.[1] Others obtained larger transverse velocity than the longitudinal one that the daughter particles indeed accelerated after fragmentation, as shown in figure 3(*b*,*e*). In some events, one of the daughter particles further broke into two pieces, as shown in figure 3(*c*,*f*). Note that one trajectory of the particle after the fragmentation event (figure 3*c*-ii) was too short to follow and thus was neglected in the analysis. These motions of particles were associated with not only the size but also the local plasma conditions.

The normalized mass loss $L = (m_0 - m_1 - m_2)/m_0$ during the fragmentation and the mass ratio $R = m_1/m_2$ of two daughter particles for the events shown in figures 1 and 3 can be estimated based on momentum conservation, where m_0 is the mass of the initial dust particle and $m_{1,2}$ are the mass of the daughter particles. The results are listed in table 1. The errors are caused by the uncertainties of the high-speed camera. It is assumed to be one-quarter of a pixel, which may be exaggerated. Except for the event shown in figure 3(*d*), the estimated mass ratio is close to unity, indicating that two daughter particles have similar size. Note that the negative mass loss may be a measurement error, caused by the low temporal resolution of the recording. (Actually, L is expected to be positive due to jetting associated with droplet breakup and small fragments which may be invisible to the camera.)

[1]Note that in figure 3(*d*), the trajectory of one fragment (the upper one) is similar to that of the parent dust, resulting in an extreme mass ratio between two fragments. Meanwhile, the other fragment (the lower one) appears much dimmer. It is possible that the second dust does not result from the fragmentation but emerges as a separate dust.

https://doi.org/10.1017/S0022377823000260 Published online by Cambridge University Press

Figure	Shot	m_1/m_0	m_2/m_0	L (%)	R
1	46618	0.40 ± 0.10	0.51 ± 0.10	9.17 ± 13.76	0.93 ± 0.10
3(*a*)	46617	0.67 ± 0.18	0.38 ± 0.20	-5.07 ± 27.22	1.20 ± 0.24
3(*b*)	46618	0.59 ± 0.34	0.28 ± 0.15	12.49 ± 37.09	1.29 ± 0.33
3(*c*-i)	46617	0.63 ± 0.21	0.36 ± 0.17	0.53 ± 27.19	1.20 ± 0.23
3(*d*)	46489	0.89 ± 0.09	0.04 ± 0.12	7.44 ± 14.85	2.89 ± 3.07
3(*e*)	46542	0.46 ± 0.13	0.37 ± 0.12	16.64 ± 18.03	1.08 ± 0.16
3(*f*-i)	46618	0.54 ± 0.31	0.29 ± 0.14	16.99 ± 33.78	1.23 ± 0.30
3(*f*-ii)	46618	0.44 ± 0.15	0.47 ± 0.22	8.70 ± 26.08	0.98 ± 0.19
3(*f*-iii)	46618	0.60 ± 0.47	0.46 ± 0.29	-5.19 ± 54.89	1.09 ± 0.37

TABLE 1. The estimated parameters associated with the fragmentation events shown in figures 1 and 3. The mass loss L and mass ratio R are calculated based on momentum conservation. The errors are estimated assuming that the particle tracking has an accuracy of 1/4 pixel.

3. Numerical simulations

In order to study the dynamics of the fragments after breakup, a simple equation-of-motion simulation was applied to fit the trajectories (Block & Melzer 2019). Since the mass ratio of the daughter particles is close to unity, we assumed that they were spheres and had the same radius $a_1 = a_2$. We further assumed that those particles were made of tungsten. Two dominant forces taken into account are the electric repulsion (modelled by the screened Coulomb or Yukawa interaction potential Lampe & Joyce (2015)) and the damping force due to friction against neutral gas background (Epstein drag Epstein (1924); Baines *et al.* (1965)). The equation of motion of the daughter particles then reads

$$m\frac{\mathrm{d}\boldsymbol{v}}{\mathrm{d}t} = \boldsymbol{F}_{\mathrm{Yuk}} + \boldsymbol{F}_{\mathrm{damp}}, \tag{3.1}$$

where $\boldsymbol{F}_{\mathrm{Yuk}} = (Q_1Q_2/r^2)(1 + r/\lambda_{\mathrm{D}})\exp(-r/\lambda_{\mathrm{D}})$ is the Yukawa repulsive force, r is the interparticle distance, λ_{D} is the Debye length and $\boldsymbol{F}_{\mathrm{damp}}$ is the damping force.

As an example, here we simulated the trajectories of the fragmentation event in figure 1. The temperature and density are set as $T_{\mathrm{e}} = T_{\mathrm{i}} = 200$ eV and $n_{\mathrm{e}} = n_{\mathrm{i}} = 10^{13}$ cm^{-3}, respectively, resulting in a Debye length $\lambda_{\mathrm{D}} \approx 24$ μm. Before the fragmentation, the dust particle was assumed to rotate with an angular velocity $\omega = 10^7$ rad s^{-1} and the initial velocity was 150 m s^{-1}. The charge of the particle was calculated with the orbital motion limited theory (Allen 1992). The electron and ion collection and the thermal emission were taken into account. The charge of the particle Q can be described as

$$\frac{\mathrm{d}Q}{\mathrm{d}t} = I_{\mathrm{e}} - I_{\mathrm{i}} - I_{\mathrm{th}} \tag{3.2}$$

where $I_{\mathrm{e}} = \sqrt{8\pi}a^2 n_{\mathrm{e}} v_{\mathrm{Te}} \exp(-z)$ is the electron current, $I_{\mathrm{i}} = \sqrt{8\pi}n_{\mathrm{i}}a^2 v_{\mathrm{Ti}}(1 + z)$ is the ion current, $v_{\mathrm{Te}} = \sqrt{T_{\mathrm{e}}/m_{\mathrm{e}}}$ is the electron thermal velocity, $v_{\mathrm{Ti}} = \sqrt{T_{\mathrm{i}}/m_{\mathrm{i}}}$ is the ion thermal velocity, $I_{\mathrm{th}} = 4\pi a^2 A_{\mathrm{eff}} T_{\mathrm{s}}^2 \exp(-W_{\mathrm{f}}/k_{\mathrm{B}}T_{\mathrm{s}})$ is the thermal emission, $A_{\mathrm{eff}} = 60$ A cm^{-2} K^{-2} is the effective Richardson constant, T_{s} is the temperature of the dust surface and $W_{\mathrm{f}} = 4.55$ eV is the work function of tungsten (Delzanno, Lapenta & Rosenberg 2004; Komm *et al.* 2020; Tolias *et al.* 2020). The reduced particle charge z can be calculated for the spherical particle as $z = |Q|e/aT_{\mathrm{e}}$. Here it is assumed that the charge is negative. In the simulations, six surface temperatures above the tungsten melting temperature were

https://doi.org/10.1017/S0022377823000260 Published online by Cambridge University Press

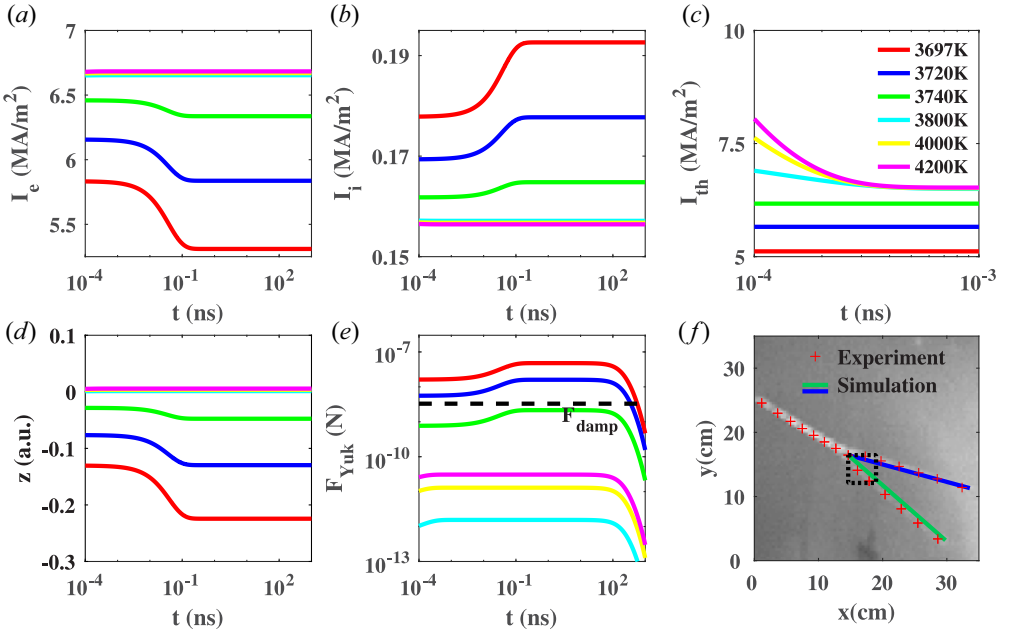

FIGURE 4. Equation-of-motion simulations of dust particles after fragmentation. (*a–c*) The electron and ion currents and the thermal emission, where colours represent different surface temperature T_s. (*d*) The reduced charges z of the particles. (*e*) The interaction force and damping force exerted on the daughter particle in the initial stage, highlighted by the dotted rectangle in (*f*) where the trajectories of relatively large particles in experiment (red plus) and simulations (blue and green lines) are shown. For different surface temperature of the dust particles, the trajectories are indistinguishable in the simulations.

selected and calculated. For high surface temperature, the dust charge is positive. The dust can recapture the thermionic electrons, resulting in a factor $(1 - zT_e/T_s)\exp(zT_e/T_s)$ in the thermal emission currents (Vignitchouk, Tolias & Ratynskaia 2014; Autricque *et al.* 2017). Aslo z-containing factors in the expressions for ion and electron currents should be interchanged. But since z is very close to zero in this case (figure 4d), this does not result in any appreciable effect. Here, slight magnetization of electron collection and thin sheath effects on ion collection were neglected in our simulations (Vignitchouk, Ratynskaia & Tolias 2017).

The initial charge of each daughter particle was set as half the value of the particle charge before fragmentation. As soon as the fragmentation occurred, the two daughter particles acquired additional velocity due to the rotation and moved in opposite directions with an initial relative velocity $\sim$36 m s^{-1} with respect to the centre of mass.[2] The two daughter particles were recharged by the electron and ion current and the thermal emission in the plasma during the transport. The electron and ion current and the thermal emission also evolved as the particle was recharged, as shown in figure 4. By varying the angle α between particle velocity direction and fragmentation direction, we fit the particle trajectories in the simulations to the experimental observations. As a result of the fit, an angle $\alpha \sim 57^\circ$ was obtained and the radius of the dust particle before fragmentation was $\sim$10 μm. It turns out that the particle trajectories are indistinguishable for different surface temperature, as

[2]The initial relative velocity was assumed based on the conservation of momentum of the particles before and after the fragmentation.

https://doi.org/10.1017/S0022377823000260 Published online by Cambridge University Press

shown in figure 4(f). The acquired initial velocities of the daughter particles from the rotation play an essential role in their trajectories after fragmentation.

4. Discussion

The essential physics behind the instability of a charged liquid particle is relatively simple. The inward restoring force per unit area associated with the surface tension is $F_{\mathrm{st}} = 2\gamma/a$ (Landau & Lifshitz 1980). If electrical charge is present on the surface of such a sphere, an outward force ('negative pressure') is exerted on the surface (Landau & Lifshitz 1984). The magnitude of this force is $F_{\mathrm{el}} = \frac{1}{2}\sigma E = Q^2/(8\pi a^4)$, where $\sigma = Q/4\pi a^2$ is the charge surface density and $E = Q/a^2$ is the electric field. If $F_{\mathrm{el}} > F_{\mathrm{st}}$, the outward electric force cannot be compensated by the inward surface tension force and the droplet becomes unstable. This results in the well-known Rayleigh instability criterion $Q^2 > 16\pi a^3\gamma$ (Rayleigh 1882). If we take the rotational effect into account, an additional centrifugal force $F_{\mathrm{ce}} = a^2\rho\omega^2/4$ points outwards, where ρ is the mass density of the particle. Then the instability condition becomes $F_{\mathrm{el}} + F_{\mathrm{ce}} > F_{\mathrm{st}}$. For the plasma parameters assumed in § 3, the instability condition is fulfilled and the fragmentation of the dust particle happens, which agrees with our experimental results. The underlying mechanism leading to the high angular velocities has not been identified yet and is the subject of much speculation (Ratynskaia, Vignitchouk & Tolias 2022*b*).

5. Conclusion

To summarize, we have described the spontaneous fragmentation of dust particles in magnetic confinement fusion in this article. Multiple fragmentation events were observed in the EAST and the trajectories were recorded using a high-speed camera. The size ratio of the daughter particles has been estimated based on momentum conservation. Equation-of-motion simulations have been performed to study the particle dynamics after fragmentation. The simulation results are consistent with the experimental observations. Our results show that the surface temperature of the dust particles plays a significant role in the charging and the particle interaction. However, the trajectories of the fragments mainly depend on their acquired initial velocities after fragmentation.

In future, we plan to conduct a statistical study of dust disintegration systematically and install an infrared camera to the EAST to measure the temperatures directly in the experiments.

Acknowledgements

The authors thank the referees for the valuable comments to improve the quality of this article.

Editor Edward Thomas, Jr. thanks the referees for their advice in evaluating this article.

Funding

This work was supported by the National Natural Science Foundation of China (grant numbers 12035003 and 11975073); the National Key R&D Program of China (grant number 2017YFE0301104); and Fundamental Research Funds for the Central Universities (grant number 2232023G-10).

Declaration of interests

The authors report no conflict of interest.

https://doi.org/10.1017/S0022377823000260 Published online by Cambridge University Press

Data availability statement

The data that support the findings of this study are available from the corresponding author upon reasonable request.

REFERENCES

ACHTZEHN, T., MÜLLER, R., DUFT, D. & LEISNER, T. 2005 The coulomb instability of charged microdroplets: dynamics and scaling. *Eur. Phys. J.* D **34**, 311–313.

ALLEN, J.E. 1992 Probe theory – the orbital motion approach. *Phys. Scr*. **45** (5), 497–503.

ARNAS, C., IRBY, J., CELLI, S., DE TEMMERMAN, G., ADDAB, Y., COUËDEL, L., GRISOLIA, C., LIN, Y., MARTIN, C., PARDANAUD, C., *et al.* 2017 Characterization and origin of large size dust particles produced in the Alcator C-Mod tokamak. *Nucl. Mater. Energy* **11**, 12–19.

AUTRICQUE, A., FEDORCZAK, N., KHRAPAK, S.A., COUËDEL, L., KLUMOV, B., ARNAS, C., NING, N., LAYET, J.-M. & GRISOLIA, C. 2017 Magnetized electron emission from a small spherical dust grain in fusion related plasmas. *Phys. Plasmas* **24** (12), 124502.

AUTRICQUE, A., KHRAPAK, S.A., COUËDEL, L., FEDORCZAK, N., ARNAS, C., LAYET, J.-M. & GRISOLIA, C. 2018 Electron collection and thermionic emission from a spherical dust grain in the space-charge limited regime. *Phys. Plasmas* **25** (6), 063701.

BAINES, M.J., WILLIAMS, I.P., ASEBIOMO, A.S. & AGACY, R.L. 1965 Resistance to the motion of a small sphere moving through a gas. *Mon. Not. R. Astron. Soc*. **130** (1), 63–74.

BLOCK, D. & MELZER, A. 2019 Dusty (complex) plasmas—routes towards magnetized and polydisperse systems. *J. Phys.* B **52** (6), 063001.

CHEN, S., ZHONG, F., YANG, Q., LI, L., LIANG, Y., ZHANG, B. & HU, L. 2019 Parametric dependence of type-I and type-III ELMS and dynamic characteristics for ELM filaments in EAST tokamak. *IEEE Trans. Plasma Sci*. **47** (1), 799–806.

COPPINS, M. 2010 Electrostatic breakup in a misty plasma. *Phys. Rev. Lett*. **104**, 065003.

DELZANNO, G.L., LAPENTA, G. & ROSENBERG, M. 2004 Attractive potential around a thermionically emitting microparticle. *Phys. Rev. Lett*. **92**, 035002.

DELZANNO, G.L. & TANG, X. 2014 Survivability of dust in tokamaks: dust transport in the divertor sheath. *Phys. Plasmas* **21** (2), 022502.

DUFT, D., LEBIUS, H., HUBER, B.A., GUET, C. & LEISNER, T. 2002 Shape oscillations and stability of charged microdroplets. *Phys. Rev. Lett*. **89**, 084503.

EPSTEIN, P.S. 1924 On the resistance experienced by spheres in their motion through gases. *Phys. Rev*. **23**, 710–733.

FORTOV, V.E., IVLEV, A.V., KHRAPAK, S.A., KHRAPAK, A.G. & MORFILL, G.E. 2005 Complex (dusty) plasmas: current status, open issues, perspectives. *Phys. Rep* **421**, 1–103.

GRISOLIA, C., ROSANVALLON, S., SHARPE, PH. & WINTER, J. 2009 Micro-particles in ITER: a comprehensive review. *J. Nucl. Mater*. **386–388**, 871–873.

HOLGATE, J.T. & COPPINS, M. 2018 Shapes, stability, and hysteresis of rotating and charged axisymmetric drops in a vacuum. *Phys. Fluids* **30** (6), 064107.

HOLGATE, J.T., SIMONS, L., ANDREW, Y. & STAVROU, C.K. 2019 Spontaneous rapid rotation and breakup of metal droplets in tokamak edge plasmas. *Europhys. Lett*. **127** (4), 45004.

HUTCHINSON, I.H. 2004 Spin stability of asymmetrically charged plasma dust. *New J. Phys*. **6**, 43.

JIA, M., YANG, Q., ZHONG, F., ZENG, A., LU, H. & SHU, S. 2015 A tangentially visible fast imaging system on EAST. *Plasma Sci. Technol*. **17** (12), 991–995.

KEILHACKER, M., BECKER, G., BERNHARDI, K., EBERHAGEN, A., ELSHAER, M., FUBMANN, G., GEHRE, O., GERNHARDT, J. & GIERKE, G.V. 1984 Confinement studies in L and H-type Asdex discharges. *Plasma Phys. Control. Fusion* **26** (1A), 49–63.

KOMM, M., RATYNSKAIA, S., TOLIAS, P. & PODOLNIK, A. 2020 Space-charge limited thermionic sheaths in magnetized fusion plasmas. *Nucl. Fusion* **60** (5), 054002.

KOROMYSLOV, V.A., GRIGOR'EV, A. & RYBAKOVA, M. 2002 Disintegration of a drop in an external electrostatic field. *Tech. Phys*. **47**, 682–689.

KRASHENINNIKOV, S.I. 2006 On dust spin up in uniform magnetized plasma. *Phys. Plasmas* **13** (11), 114502.

https://doi.org/10.1017/S0022377823000260 Published online by Cambridge University Press

KRASHENINNIKOV, S.I., TOMITA, Y., SMIRNOV, R.D. & JANEV, R.K. 2004 On dust dynamics in tokamak edge plasmas. *Phys. Plasmas* **11** (6), 3141–3150.

LAMPE, M. & JOYCE, G. 2015 Grain-grain interaction in stationary dusty plasma. *Phys. Plasmas* **22** (2), 023704.

LANDAU, L.D. & LIFSHITZ, E.M. 1980 *Statistical Physics*. Butterworth-Heinemann.

LANDAU, L.D. & LIFSHITZ, E.M. 1984 *Electrodynamics of Continuous Media*. Butterworth-Heinemann.

LAUX, M., BALDEN, M. & SIEMROTH, P. 2014 Modification of arc emitted W particles in a model scrape-off layer plasma. *Phys. Scr*. **2014** (T159), 014026.

LIAO, L. & HILL, R.J.A. 2017 Shapes and fissility of highly charged and rapidly rotating levitated liquid drops. *Phys. Rev. Lett*. **119**, 114501.

LI, J., GUO, H.Y., WAN, B.N., GONG, X.Z., LIANG, Y.F., XU, G.S., GAN, K.F., HU, J.S., WANG, H.Q., WANG, L., *et al.* 2013 A long-pulse high-confinement plasma regime in the experimental advanced superconducting tokamak. *Nat. Phys*. **9** (12), 817–821.

LIU, J., CHEN, L., MAO, A., SUN, G. & DUAN, P. 2013 Charging, movement and lifetime characteristics of dust in magnetic fusion devices. *Vacuum* **88**, 177–181.

LUNSFORD, R., SUN, Z., MAINGI, R., HU, J.S., MANSFIELD, D., XU, W., ZUO, G.Z., DIALLO, A., OSBORNE, T., TRITZ, K., *et al.* 2018 Injected mass deposition thresholds for lithium granule instigated triggering of edge localized modes on EAST. *Nucl. Fusion* **58** (3), 036007.

MORFILL, G.E. & IVLEV, A.V. 2009 Complex plasmas: an interdisciplinary research field. *Rev. Mod. Phys*. **81**, 1353–1404.

PAN, H., DING, R., PENG, J., YAN, R., ZHU, D. & CHEN, J. 2022 Characterization of dust produced during the 2021 first campaign in EAST tokamak. *Nucl. Mater. Energy* **33**, 101251.

PARDANAUD, C., DELLASEGA, D., PASSONI, M., MARTIN, C., ROUBIN, P., ADDAB, Y., ARNAS, C., COUËDEL, L., MINISSALE, M., SALOMON, E., *et al.* 2020 Post-mortem analysis of tungsten plasma facing components in tokamaks: Raman microscopy measurements on compact, porous oxide and nitride films and nanoparticles. *Nucl. Fusion* **60** (8), 086004.

RATYNSKAIA, S., BORTOLON, A. & KRASHENINNIKOV, S.I. 2022*a* Dust and powder in fusion plasmas: recent developments in theory, modeling, and experiments. *Rev. Mod. Plasma Phys*. **6** (1), 20.

RATYNSKAIA, S., CASTALDO, C., BERGSÅKER, H. & RUDAKOV, D. 2011 Diagnostics of mobile dust in scrape-off layer plasmas. *Plasma Phys. Control. Fusion* **53** (7), 074009.

RATYNSKAIA, S., THORÉN, E., TOLIAS, P., PITTS, R.A., KRIEGER, K., VIGNITCHOUK, L., IGLESIAS, D., THE ASDEX-UPGRADE TEAM, THE JET CONTRIBUTORS, THE EUROFUSION MST1 TEAM 2020 Resolidification-controlled melt dynamics under fast transient tokamak plasma loads. *Nucl. Fusion* **60** (10), 104001.

RATYNSKAIA, S., TOLIAS, P., BYKOV, I., RUDAKOV, D., DE ANGELI, M., VIGNITCHOUK, L., RIPAMONTI, D., RIVA, G., BARDIN, S., VAN DER MEIDEN, H., *et al.* 2016 Interaction of adhered metallic dust with transient plasma heat loads. *Nucl. Fusion* **56** (6), 066010.

RATYNSKAIA, S., TOLIAS, P., DE ANGELI, M., ROHDE, V., HERRMANN, A., RIPAMONTI, D., RIVA, G., THORÉN, E., VIGNITCHOUK, L., SIEGLIN, B., *et al.* 2018 Interaction of metal dust adhered on castellated substrates with the ELMy H-mode plasmas of ASDEX-upgrade. *Nucl. Fusion* **58** (10), 106023.

RATYNSKAIA, S., VIGNITCHOUK, L. & TOLIAS, P. 2022*b* Modelling of dust generation, transport and remobilization in full-metal fusion reactors. *Plasma Phys. Control. Fusion* **64** (4), 044004.

RAYLEIGH, LORD 1882 XX. On the equilibrium of liquid conducting masses charged with electricity. *Phil. Mag*. **14** (87), 184–186.

SHALPEGIN, A., BROCHARD, F., RATYNSKAIA, S., TOLIAS, P., DE ANGELI, M., VIGNITCHOUK, L., BYKOV, I., BARDIN, S., BYSTROV, K., MORGAN, T., *et al.* 2015 Highly resolved measurements of dust motion in the sheath boundary of magnetized plasmas. *Nucl. Fusion* **55** (11), 112001.

SHARPE, P., PETTI, D. & BARTELS, H.-W. 2002 A review of dust in fusion devices: implications for safety and operational performance. *Fusion Engng Des*. **63**, 153–163.

TOLIAS, P., KOMM, M., RATYNSKAIA, S. & PODOLNIK, A. 2020 Origin and nature of the emissive sheath surrounding hot tungsten tokamak surfaces. *Nucl. Mater. Energy* **25**, 100818.

Tolias, P., Ratynskaia, S., De Angeli, M., De Temmerman, G., Ripamonti, D., Riva, G., Bykov, I., Shalpegin, A., Vignitchouk, L., Brochard, F., *et al.* 2016 Dust remobilization in fusion plasmas under steady state conditions. *Plasma Phys. Control. Fusion* **58** (2), 025009.

Vignitchouk, L., Ratynskaia, S. & Tolias, P. 2017 Analytical model of particle and heat flux collection by dust immersed in dense magnetized plasmas. *Plasma Phys. Control. Fusion* **59** (10), 104002.

Vignitchouk, L., Tolias, P. & Ratynskaia, S. 2014 Dust–wall and dust–plasma interaction in the migraine code. *Plasma Phys. Control. Fusion* **56** (9), 095005.

Wan, B., Li, J., Guo, H., Liang, Y., Xu, G., Wang, L., Gong, X., Garofalo, A., for the EAST Team Collaborators 2015 Advances in H-mode physics for long-pulse operation on EAST. *Nucl. Fusion* **55** (10), 104015.

Wang, L., Guo, H.Y., Xu, G.S., Liu, S.C., Gan, K.F., Wang, H.Q., Gong, X.Z., Liang, Y., Zou, X.L., Hu, J.S., *et al.* 2014 Scaling of divertor power footprint width in RF-heated type-III ELMy H-mode on the EAST superconducting tokamak. *Nucl. Fusion* **54** (11), 114002.

Winter, J. 1999 Dust in fusion devices – experimental evidence, possible sources and consequences. *Plasma Phys. Control. Fusion* **40**, 1201.